Development 138, 1409-1419 (2011) doi:10.1242/dev.060046

A Slit/miR-218/Robo regulatory loop is required during heart tube formation in zebrafish

Jason E. Fish[1,2,3,4,*,†], Joshua D. Wythe[1,5,6,*], Tong Xiao[7], Benoit G. Bruneau[1,5,6], Didier Y. R. Stainier[2,6], Deepak Srivastava[1,2,5] and Stephanie Woo[2,6,†]

SUMMARY

Members of the Slit family of secreted ligands interact with Roundabout (Robo) receptors to provide guidance cues for many cell types. For example, Slit/Robo signaling elicits repulsion of axons during neural development, whereas in endothelial cells this pathway inhibits or promotes angiogenesis depending on the cellular context. Here, we show that miR-218 is intronically encoded in *slit2* and *slit3* and that it suppresses Robo1 and Robo2 expression. Our data indicate that miR-218 and multiple Slit/Robo signaling components are required for heart tube formation in zebrafish and that this network modulates the previously unappreciated function of Vegf signaling in this process. These findings suggest a new paradigm for microRNA-based control of ligand-receptor interactions and provide evidence for a novel signaling pathway regulating vertebrate heart tube assembly.

KEY WORDS: Slit/Robo, Vegf, MicroRNA, Heart tube formation, Zebrafish

INTRODUCTION

During vertebrate cardiac morphogenesis, myocardial and endocardial precursors are specified in two bilateral domains within the anterior lateral plate mesoderm and subsequently migrate toward the embryonic midline, where they fuse into a linear heart tube consisting of an outer ring of cardiomyocytes surrounding an inner core of endocardial cells (Bussmann et al., 2007; Holtzman et al., 2007). Analysis of several zebrafish mutants has shed light on the requirements for myocardial migration, including the specification and development of the endoderm (Alexander et al., 1999), the deposition of extracellular matrix proteins such as fibronectin (Trinh and Stainier, 2004; Sakaguchi et al., 2006) and signaling through both heterotrimeric G proteins (Kupperman et al., 2000; Osborne et al., 2008) and Rho family GTPases (D'Amico et al., 2007). By contrast, much less is known about the mechanisms that control endocardial migration. For example, in embryos mutant for the transcription factor Scl/Tal1, endocardial cells migrate to the midline but then fail to migrate posteriorly, resulting in endocardial cell aggregation at the arterial pole (Bussmann et al., 2007). Importantly, midline-derived cues that guide endocardial (or myocardial) cells towards the midline have not been identified.

Several guidance molecules are expressed at the embryonic midline, including the Slit family of secreted extracellular matrix proteins. Although Slits and their Roundabout (Robo) receptors were initially characterized as repulsive guidance cues for neuronal axons (Kidd et al., 1998a; Kidd et al., 1999), they are also involved in the development of several other organs systems (Liu et al., 2003; Grieshammer et al., 2004; Strickland et al., 2006). In *Drosophila*, Slit functions via Robo1/2 as a repulsive cue to position cardioblasts relative to the midline (Qian et al., 2005). Subsequently, Slit/Robo signaling is required to downregulate E-cadherin cell-surface localization during lumenization of the heart tube (Medioni et al., 2008; Santiago-Martinez et al., 2008). It is unclear whether these observations can be extended to vertebrates, considering that *Drosophila* lacks the endocardium, which is required for vertebrate heart tube assembly (Holtzman et al., 2007).

In vertebrates, the Robo family comprises four known members (Robo1-4), whereas the Slit family has three members (Slit1-3). Here, we show that a highly conserved microRNA, miR-218, is encoded intronically in *slit2* and *slit3* and negatively regulates Robo1 and Robo2. Knockdown experiments indicate that Slit2, Robo1 and miR-218 are required for the formation of the linear heart tube in zebrafish. Further analyses indicate that Vegf is also required for migration of the heart fields to the midline, and that Slit/Robo signaling regulates the response of endocardial cells to Vegf. Thus, we provide evidence that a novel Slit/miR-218/Robo/Vegf signaling axis controls heart tube formation in zebrafish.

MATERIALS AND METHODS

Plasmids

HA-tagged rat ROBO1 (Li et al., 1999) and Myc-tagged rat ROBO1 (Stein and Tessier-Lavigne, 2001) have been described previously. mCherry was from Timothy Gomez (University of Wisconsin, Madison).

Morpholinos (MOs)

MOs (Gene Tools or Open Biosystems) were titrated to avoid toxic effects of excess MO.

Control MO, CCTCTTACCTCAGTTACAATTTATA;
miR-218 MO[1], TGCATGGTTAGATCAAGCACAAGGG;
miR-218 MO[2], CACATGGTTAGATCAAGCACAAGGG;
robo1 ATG MO, ATCCAATTATTCTCCCCGTCATCGT (Devine and Key, 2008);
robo4 ATG MO, GCAGACACCTGCATCTTCAGCCTAA;
slit2 ATG MO, GCACCACTGATTTCAACACAAACAT;
slit3 ATG MO, CCCCCAATACTTTACCCACCGCATC; and

[1]Gladstone Institute of Cardiovascular Disease, San Francisco, CA 94158, USA. [2]Department of Biochemistry and Biophysics, University of California, San Francisco, CA 94158, USA. [3]Toronto General Research Institute, University Health Network, Toronto, ON M5G 1L8, Canada. [4]Department of Laboratory Medicine and Pathobiology, University of Toronto, Toronto, ON M5G 1L8, Canada. [5]Department of Pediatrics, University of California, San Francisco, CA 94143, USA. [6]Cardiovascular Research Institute, University of California, San Francisco, CA 94143, USA. [7]Department of Physiology, University of California, San Francisco, CA 94143, USA.

*These authors contributed equally to this work
†Authors for correspondence (jason.fish@utoronto.ca; stephanie.woo@ucsf.edu)

Accepted 12 January 2011

vegfa ATG MO, CTCGTCTTATTTCCGTGACTGTTTT (Ober et al., 2004).

Zebrafish embryology, MO injections and drug treatment

Tg(kdrl:ras-mCherry)^{s896} (Chi et al., 2008), *Tg(myl7:GFP)*^{twu26} (Huang et al., 2003), *Tg(kdrl:GFP)*^{s843} (Jin et al., 2007), *Tg(gata1:dsRED)*^{sd2} (Traver et al., 2003) and *Tg(sox17:GFP)*^{s870} (Chung and Stainier, 2008) zebrafish lines were used in these studies. Embryos were injected at the 1-cell stage with 8-12 ng of *miR-218* MO^1, 5-10 ng of *miR-218* MO^2, 4 ng *robo1* MO, 1 ng *robo4* MO, 2 ng *slit2* MO, 3 ng *slit3* MO or 2.5 ng *vegfa* MO. For gene interaction studies, sub-phenotypic doses of *robo1* (2 ng) and *vegfa* (1 ng) MOs were used in combination, and for rescue experiments sub-phenotypic doses of *robo1* MO (1 ng) were used in combination with a phenotypic dose of *miR-218* MO^1 (12 ng). To inhibit Vegf receptor signaling, embryos were treated with the indicated concentration of Vatalanib (LC Laboratories) in embryo water. After transient pulses of the drug, embryos were washed extensively in embryo medium and allowed to develop until analyzed. To better visualize the embryos, pigment development was inhibited with 0.003% phenylthiourea.

Slit2 heat-shock experiments

Tg(hsp70l:slit2-GFP)^{rw015a} zebrafish (Yeo et al., 2004) were crossed to the *Tg(kdrl:ras-mCherry)*^{sd2} line. At the 5-somite stage, embryos were heat shocked for 1 hour at 38°C then returned to 28.5°C and raised until the 20-somite stage. Embryos were fixed and endocardial morphology was assessed by confocal microscopy as described below.

Robo1 overexpression experiments

Rat *Robo1* mRNA was synthesized from pSecTag2-*Robo1-Myc* with T7 polymerase (mMessage mMachine Kit, Ambion) and 75 pg of mRNA was injected. As a control, a similar amount of *mCherry* mRNA was injected in parallel.

Confocal and fluorescence microscopy and time-lapse analysis

For live time-lapse imaging, embryos were injected with the indicated MO and allowed to develop at 25°C until 15-16 somites. They were then embedded in 1% low-melting-point agarose and imaged at 25°C on a Nikon C1si spectral confocal microscope with a 40×/0.8 NA NIR Apo water-dipping lens. Every 5 minutes, *z*-stacks of 20-30 sections at 4-μm intervals were acquired. Images were denoised in collaboration with John Sedat (UCSF) with software developed by Jerome Boulanger (Kervrann and Boulanger, 2006). Default parameters were used, except for the patch size, which was 5×5 pixels for the mCherry channel and 8×8 pixels for the GFP channel. Maximum projections were made using ImageJ (NIH). Cell migration parameters were quantified using the Manual Tracking plug-in in ImageJ. For fixed embryos, 4% paraformaldehyde was used (4°C overnight), and embryos were processed for indirect immunofluorescence. Embryos were imaged on a Zeiss LSM 5 confocal microscope with a 40×/0.75 NA Achroplan water-dipping lens. For analysis of axial vasculature and heart structure, fixed 48 hours post-fertilization (hpf) embryos were embedded in 1% low-melting-point agarose and sectioned with a Vibratome (250-μm sections). Confocal imaging was performed as above. For analysis of cardiovascular function, live 48 hpf embryos were embedded in 1% low-melting-point agarose and movement of *Tg(gata1:*dsRed*)*^{sd2}-positive cells was observed. Images of live zebrafish were acquired using a Leica MZ16F microscope with a DFC500 camera.

In situ hybridization

Fluorescent in situ hybridization was performed as described (Schoenebeck et al., 2007) using riboprobes for *slit2* (Hutson and Chien, 2002), *robo1* (Lee et al., 2001) and *robo4* (Bedell et al., 2005). miR-218 in situ hybridization was performed as described (Sweetman et al., 2006) using a double DIG-labeled *miR-218a* LNA probe (Exiqon).

Fluorescence-activated cell sorting (FACS)

FACS was performed essentially as described (Fish et al., 2008). Embryos were manually dechorionated at the 18- to 20-somite stage and digested to a single-cell suspension with TrypLE (Invitrogen). Total RNA was isolated from cell pellets (RNeasy Micro Kit, Qiagen).

Sprouting assays

Tg(kdrl:GFP) embryos were fixed at the 26-somite stage. Embryos were immunostained with F59 (Developmental Studies Hybridoma Bank) to visualize the somites and with anti-GFP (Invitrogen) to label the blood vessels. The number of intersomitic vessel sprouts present from somites 4-16 (starting from the head and moving posteriorly) and the number of sprouts crossing the myoseptum were quantified.

Transfection and electroporation of plasmids, siRNAs and microRNA mimics

HeLa cells (ATCC) were transfected using Lipofectamine 2000 (Invitrogen) and HUVEC (ScienCell) were electroporated using the Amaxa Nucleofector according to the manufacturer's recommendations. For transfection of endothelial cells with *miR-218* mimics (20 nM), RNAi Max (Invitrogen) was used. Cells were analyzed at 48 hours post-transfection. For small interfering RNA (siRNA)-mediated knockdown of *ROBO1* and *ROBO4*, SilencerSelect siRNAs (50-100 nM, Ambion) were used.

Cell treatments

Recombinant human SLIT2-N and VEGF were purchased from PeproTech and BD Biosciences, respectively. HUVEC were serum-starved overnight in basal medium with 0.1% BSA and pretreated with 10 nM SLIT2-N for 1 hour or were left untreated, followed by stimulation with 10 ng/ml VEGF for 10 minutes.

Migration and scratch wound assays

The migration of endothelial cells was assessed as described (Fish et al., 2008).

Cell polarity experiments

After 16 hours of migration in a scratch wound assay, HUVEC were immunostained for Gigantin (Abcam) and were counterstained with FITC-phalloidin (Invitrogen) and DAPI. The position of the Golgi apparatus (Gigantin staining) with respect to the nucleus was determined. Cells in which the Golgi was less than 45° from the wound face were classified as being oriented towards the wound.

ROBO1 rescue of *miR-218* mimic-transfected cells

HUVEC (0.5×10^6) were electroporated with 2.5 μg of control or *Robo1* expression plasmids with the Amaxa Nucleofection apparatus. After 24 hours, cells were transfected with control or *miR-218* mimics (20 nM, Dharmacon) using RNAiMax (Invitrogen). Cells were analyzed 48 hours later.

Luciferase assays

Confirmation of the targeting of *robo1/ROBO1*, *robo2/ROBO2* and *srgap2/SRGAP2* by miR-218 was performed as described (Fish et al., 2008). Mutagenesis of the predicted microRNA seed sequence in *robo1/ROBO1* and *robo2/ROBO2* was performed using the QuikChange Site-Directed Mutagenesis Kit (Stratagene). The miR-218 seed sequence UGUGCUU was mutated to UGACGUU.

Western blotting

Western blots were performed as described (Fish et al., 2008) using the following antibodies: anti-phospho-ERK1/2 (MAPK3/1) (Thr202/Tyr204, Cell Signaling), anti-ERK2 (Santa Cruz), anti-GAPDH (Santa Cruz), anti-ROBO1 (Abcam, ab7279), anti-phospho-VEGFR2 (KDR) (Tyr1175, Cell Signaling) and anti-VEGFR2 (Cell Signaling).

Quantification of gene expression by real-time quantitative reverse transcriptase PCR (qRT-PCR)

MicroRNA and mRNA expression analyses were performed as described (Fish et al., 2008). Primer sequences are available upon request. For absolute quantification experiments, a *miR-218* mimic, or PCR amplicons encompassing the gene of interest, were utilized to generate a standard curve. For expression analysis of zebrafish *miR-218a-1/miR-218a-2* and *miR-218b*, RNA was reverse transcribed using the QuantiMir Kit from Systems Biosciences and primers specific for *miR-218a* or *miR-218b* were utilized.

Statistical analysis

Unless otherwise stated, all experiments were performed a minimum of three times and data represent the mean ± s.e.m. Statistical analyses were performed using a Student's *t*-test, ANOVA and the Newman-Keuls post-hoc test, or a Fisher's exact test, as appropriate. $P<0.05$ was considered statistically significant.

RESULTS

miR-218 is intronically encoded in *SLIT2* and *SLIT3* and targets the SLIT receptors *ROBO1* and *ROBO2*

We found that a family of highly conserved microRNAs – miR-218-1 and miR-218-2 – is encoded intronically in *SLIT2* and *SLIT3*, respectively (Fig. 1A). Unlike in mammals, zebrafish have three genomic copies of *miR-218*. Whereas *miR-218a-1* and *miR-218a-2* are located in *slit2* and *slit3*, respectively, *miR-218b* is intergenic. Quantitative real-time PCR with primers specific to *miR-218a* or *miR-218b* revealed that *miR-218b* is expressed at ~60-fold lower levels than *miR-218a* in 20-somite stage zebrafish embryos (data not shown), suggesting that expression of *miR-218* in zebrafish is likely to be primarily directed by the *slit2* and *slit3* loci.

A bioinformatic search for potential targets of miR-218 identified conserved complementary sequences in the 3′ UTRs of *ROBO1* and *ROBO2* (Fig. 1B). Human and zebrafish *ROBO1/robo1* or *ROBO2/robo2* 3′ UTRs were sensitive to miR-218-dependent repression in luciferase assays and mutation of their miR-218 target sites alleviated this repression (Fig. 1C). Overexpression of *miR-218* in human umbilical vein endothelial cells (HUVEC) decreased endogenous *ROBO1* and *ROBO2* mRNA (Fig. 1D). ROBO1 protein levels were also decreased (Fig. 1E), whereas ROBO2 protein was undetectable in HUVEC (data not shown). These findings suggest that *SLIT2/3*-encoded miR-218 negatively regulates ROBO1/2 expression.

SLIT-ROBO Rho GTPase activating protein 2 (*SRGAP2*), a downstream component of Slit/Robo signaling, was also identified as a potential target of miR-218. In contrast to *ROBO1* and *ROBO2*, its putative target site in the 3′ UTR was not as highly conserved across phyla (see Fig. S1A in the supplementary material). However, human and zebrafish *SRGAP2/srgap2* 3′ UTRs were repressed by miR-218 in luciferase assays (see Fig. S1B in the supplementary material). Similar to other microRNAs that target multiple components of a common pathway (Fish et al., 2008; Cordes et al., 2009), miR-218 might regulate Slit/Robo signaling at multiple nodes.

Slit/Robo signaling regulates cardiovascular function in zebrafish

Examination of *miR-218* expression during zebrafish development revealed that it was upregulated at ~24 hpf and remained highly expressed at the subsequent developmental stages analyzed (Fig. 2A). In situ hybridization revealed strong expression of *miR-218* in the heart and neural tissue at 72 hpf (Fig. 2B). *miR-218* expression in neural tissue, in light of the enriched expression of the host genes *slit2* and *slit3* in these same tissues (Holmes and Niswander, 2001), further implies that miR-218a is likely to be processed from *slit2/3*. To investigate the in vivo function of miR-218, we designed two morpholinos (MOs) to knock down miR-218 expression. The first MO (*miR-218* MO^1) targeted the Drosha (Rnasen) cleavage site of miR-218a-1, miR-218a-2 and miR-218b (see Fig. S2A in the supplementary material). The second Drosha-blocking MO (*miR-218* MO^2) was more specific for miR-218a-1 and miR-218a-2 than for miR-218b (see Fig. S2A in the supplementary material), as our previous experiments revealed a lower level of expression of miR-218b (data not shown). Injection of either of these MOs at the 1- to 2-cell stage resulted in a dose-dependent knockdown of mature miR-218, without affecting *slit2* and *slit3* mRNA levels (Fig. 2C and see Fig. S2B in the supplementary material). *miR-218* MO^1-injected embryos were morphologically indistinguishable from control embryos, with the notable exception of severe pericardial edema at 48 hpf (Fig. 2D; for quantification, see Fig. S3 in the supplementary material). This same phenotype occurred at a similar penetrance in embryos injected with *miR-218* MO^2 (see Fig. S2C and, for quantification, Fig. S3 in the supplementary material). Direct visualization of blood flow revealed reduced circulation in *miR-218* MO^1 morphants at 48 hpf, although gross vascular patterning appeared normal (Fig. 2D; for quantification see Fig. S3 in the supplementary material). Injection of *miR-218* MO^2 resulted in similar circulation defects (see Fig. S2C in the supplementary material), and a small percentage of embryos also had minor vascular defects (for quantification see Fig. S3 in the supplementary material). Because of the apparent lower toxicity, we used *miR-218* MO^1 for all further phenotypic analyses.

The sprouting of the intersomitic vessels (ISVs) at 22 hpf was unperturbed in *miR-218* MO^1-injected embryos (see Fig. S4A,B in the supplementary material), and axial vessels were lumenized (see Fig. S4C in the supplementary material). We also found no evidence of hemorrhage in *miR-218* morphants (Fig. 2D; see Fig. S2C and Fig. S3 in the supplementary material). However, the hearts of *miR-218* morphants were morphologically abnormal at 48 hpf (Fig. 2E). The combination of a dysmorphic heart and pericardial edema and the absence of severe vascular defects suggested that *miR-218* might be required for cardiogenesis.

As *miR-218* is embedded within the *slit2/3* genes and directly represses Robo1 and Robo2 in vitro, we assessed the role of the ligands Slit2 and Slit3 and the receptors Robo1, Robo2 and Robo4 in zebrafish cardiovascular development. Importantly, MO-mediated knockdown of *slit2* did not affect *miR-218* expression (data not shown). At 48 hpf, *slit2* morphants had pericardial edema and circulation defects but apparently normal vascular patterning (see Fig. S5A and, for quantification, Fig. S3 in the supplementary material). By contrast, *slit3* morphants did not develop pericardial edema; however, *slit3* morphants displayed highly penetrant vascular defects, characterized primarily by missing or detached ISVs and/or dorsal longitudinal anastomotic vessels (DLAVs) (see Fig. S3 and Fig. S5A in the supplementary material). Similar to *slit2* morphants, *robo1* and *robo4* morphants also developed pericardial edema and circulation defects (see Fig. S3 and Fig. S5A in the supplementary material). By contrast, examination of *robo2* homozygous loss-of-function mutants (*astray*; ast^{ti272z}) (Fricke et al., 2001) revealed no obvious defects in the development or function of the cardiovascular system [at 72 hpf, 6% of *astray* mutants (n=18) and 7% of control embryos (n=31) had mild pericardial edema; see Fig. S5B in the supplementary material]. Sprouting angiogenesis at 22 hpf (see Fig. S4A,B in the supplementary material) and vascular patterning at 48 hpf (see Fig. S5A in the supplementary material) appeared grossly unaffected in *slit2*, *robo1* or *robo4* morphants, suggesting that these genes do not play a major role in vascular development. These data suggest that Slit2, Robo1, Robo4 and miR-218 appear to regulate cardiac development and function, whereas Slit3 participates in vascular development.

Slit/Robo signaling regulates migration of the heart fields in zebrafish

In *Drosophila*, Slit/Robo signaling is required for proper migration and alignment of cardioblasts at the midline (Qian et al., 2005; Medioni et al., 2008; Santiago-Martinez et al., 2008).

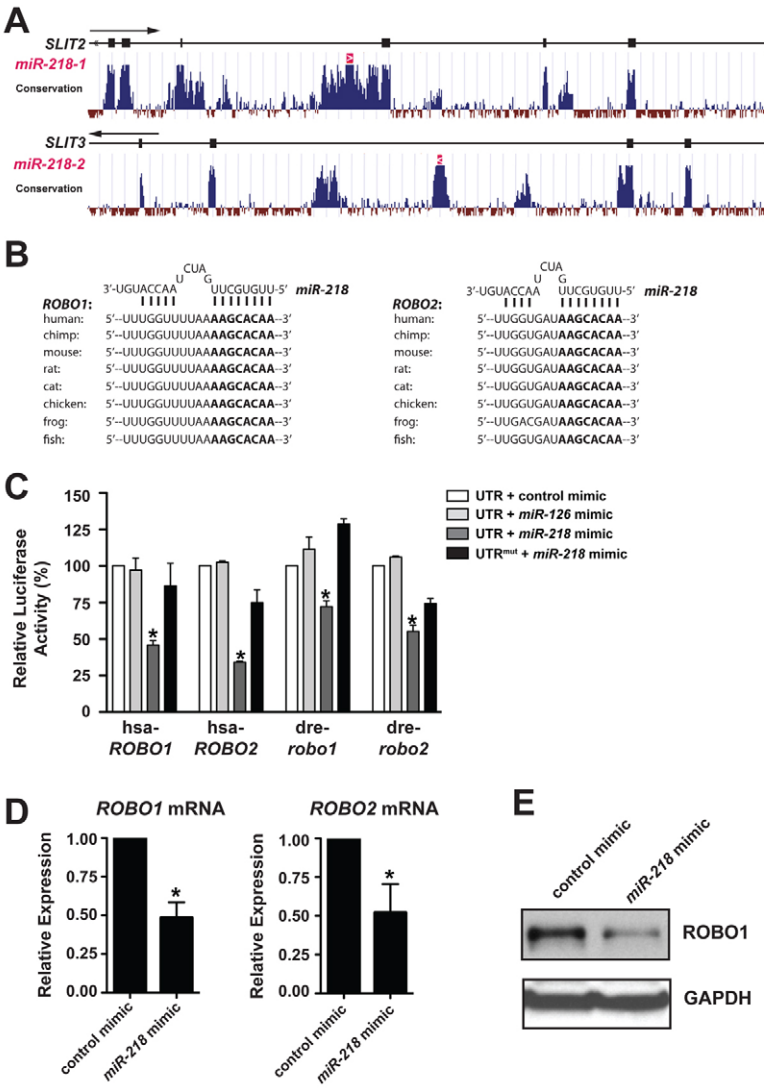

Fig. 1. *SLIT2/3*-encoded miR-218 regulates *ROBO1* and *ROBO2* expression. (**A**) Schematic of *miR-218-1* and *miR-218-2* encoding in intron 14 of human *SLIT2* and *SLIT3*, respectively (adapted from the UCSC Genome Browser) (Kent et al., 2002). Plots show the conservation of regions of genomic DNA among 18 placental mammals calculated by phyloP (Siepel et al., 2005). Exons are indicated as black boxes. *miR-218* is indicated by red boxes. The direction of transcription is indicated by arrows. (**B**) Conservation of the miR-218 binding site in *ROBO1* and *ROBO2* among various species. Sequences complementary to the miR-218 seed sequence are indicated in bold. (**C**) Luciferase assays in HeLa cells demonstrating regulation of human and zebrafish *ROBO1* and *ROBO2* by *miR-218*. *miR-126* was utilized as a control. *, $P<0.05$ compared with UTR^{mut}. (**D**) *miR-218* overexpression leads to downregulation of *ROBO1/2* mRNA in HUVEC. *, $P<0.05$ compared with control mimic. (**E**) Representative western blot demonstrates that ROBO1 levels are diminished in *miR-218*-transfected HUVEC. Data in C and D are mean + s.e.m.

Since cardiac function was impaired in Slit/Robo morphants at late developmental time points (i.e. 48 hpf), we examined whether these late defects arise from an earlier requirement for Slit/Robo signaling during heart field fusion. First, we examined the expression of several Slit/Robo signaling components by mRNA in situ hybridization at stages when the heart fields are fusing at the midline (18-20 somites; see Fig. S6A in the supplementary material). *slit2* appeared to be expressed in midline structures, including the floor plate of the neural tube. Additionally, *slit2* was expressed in the endoderm and in endocardial cells. *robo1* appeared to be expressed in the endoderm, myocardium and endocardium, whereas *robo4* expression was detected in the dorsal neural tube and at low levels in the endocardium. Quantification of *miR-218*, *slit2*, *slit3*, *robo1*, *robo2* and *robo4* expression was performed by real-time qRT-PCR analysis of FACS-isolated endothelial [*Tg(kdrl:*GFP*)*], myocardial [*Tg(myl7:*GFP*)*] or endodermal [*Tg(sox17:*GFP*)*] cells from 18- to 20-somite stage embryos (see Fig. S6B in the supplementary material). Each transcript, with the exception of *robo2*, was expressed at appreciable levels in each of these tissue types, confirming that they are present in cell types that are required for heart formation, namely the endothelium/endocardium, myocardium and endoderm.

We examined the functional role of the Slit/Robo signaling pathway in the migration of the bilateral heart fields to the midline. In vivo time-lapse confocal microscopy revealed that knockdown of *slit2* resulted in abnormal migration of endocardial cells (Fig. 3A; see Fig. S7A in the supplementary material). Individual endocardial cells migrated significantly faster in *slit2* morphants than in controls (Fig. 3B) and also exhibited a loss of directionality (Fig. 3C; see Fig. S7A and Movies 1 and 2 in the supplementary material). *slit2* knockdown also disrupted collective cell migration, as individual migrating endocardial cells did not contact neighboring cells and they extended numerous filopodia in multiple directions (Fig. 3A, arrows; see Movies 1 and 2 in the supplementary material). However, the speed (Fig. 3B) and directionality (see Fig. S7B in the supplementary material) of myocardial migration were not affected in *slit2* morphants compared with controls, suggesting that Slit2 primarily regulates endocardial migratory behavior. As a consequence of the disrupted migration of the heart fields, multiple lumens appeared to form in 43% of morphants (n=57; see Fig. S7C in the supplementary material).

In contrast to *slit2* morphants, *miR-218* knockdown reduced the migration rate of endocardial cells (Fig. 3A,B), perhaps owing to a loss of miR-218-mediated repression of the Slit receptors Robo1 and/or Robo2. Myocardial cell migration was also reduced after

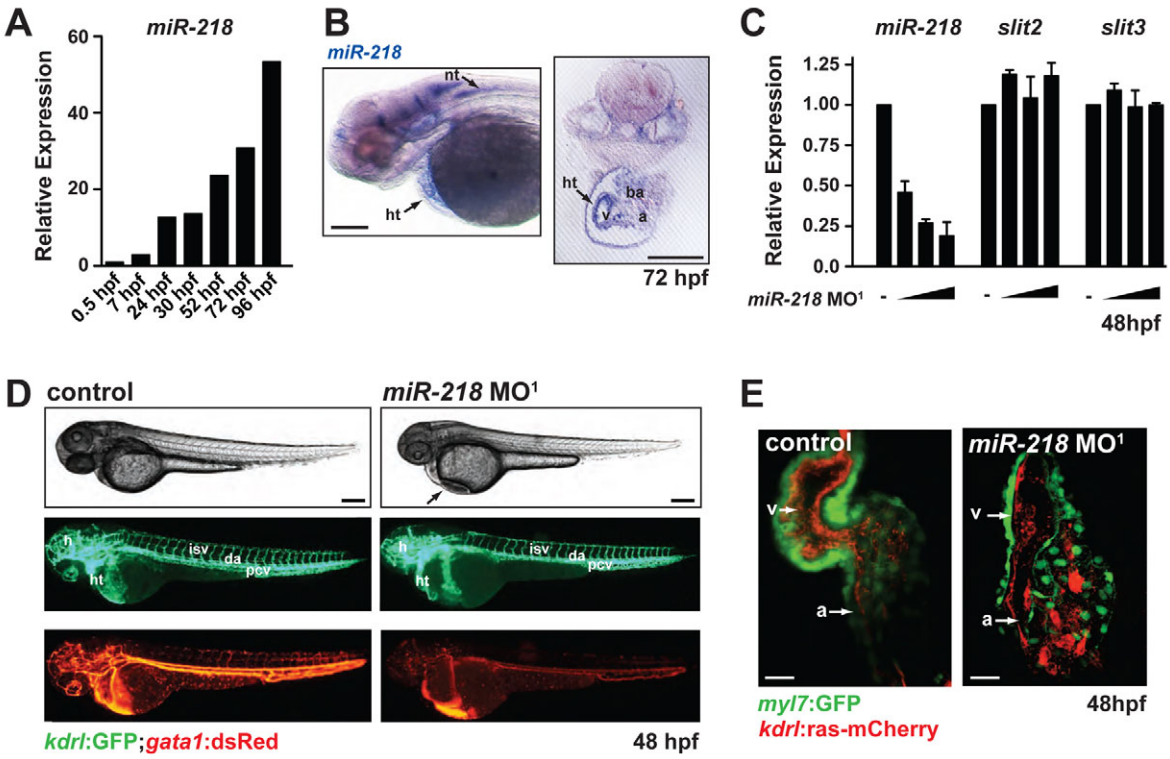

Fig. 2. *miR-218* regulates heart formation and function. (**A**) Expression of *miR-218* (relative to 0.5 hpf timepoint) was monitored by real-time qRT-PCR during zebrafish development. (**B**) In situ analysis of *miR-218* expression at 72 hpf reveals expression in the heart and neuronal tissue. (**C**) Expression of *miR-218*, *slit2* and *slit3* were quantified by real-time qRT-PCR in *miR-218* morphants (2.5, 5 and 10 ng of *miR-218* MO[1]) at 48 hpf. Data are mean + s.e.m. (**D**) Control and *miR-218* morphants were assessed at 48 hpf by live imaging of embryos. Phase-contrast images (top) demonstrate pericardial edema in the *miR-218* morphant (arrow). Fluorescent images of the same embryos show labeling of endothelial/endocardial cells in *Tg(kdrl*:GFP*)* (middle) and labeling of blood cells in *Tg(gata1*:dsRed*)* (bottom). Vascular patterning appears normal in *miR-218* morphants, but circulation is reduced. (**E**) Cardiac morphology at 48 hpf was assessed by confocal microscopy (ventral view). *Tg(myl7*:GFP*)* expression labels the myocytes and *Tg(kdrl*:ras-mCherry*)* labels the endocardium. *miR-218* morphant hearts contain myocytes and endocardium but exhibit severe morphological defects. ht, heart; nt, neural tube; a, atrium; v, ventricle; ba, branchial arches; h, head; isv, intersomitic vessel; da, dorsal aorta; pcv, posterior cardinal vein. Scale bars: 100 μm in B,D; 25 μm in E.

miR-218 knockdown (Fig. 3A,B) and these morphants showed an increase in incomplete heart field fusion at the 20-somite stage [40% of *miR-218* morphants (*n*=53) versus 8% of control embryos (*n*=125)]. Although we were unable to detect a significant change in *robo1* or *robo2* expression by qRT-PCR analysis of whole *miR-218* morphant embryos (data not shown), in situ hybridization suggested increased *robo1* expression in the endocardium and myocardium of *miR-218* morphants at the 20-somite stage (Fig. 3D). These data indicate that miR-218, potentially through its regulation of Robo1 and/or Robo2, controls heart field migration.

As *robo2* is expressed at low levels in the endocardium/myocardium and *robo2* mutants displayed no cardiovascular abnormalities, we focused our attention on the other miR-218 target, *robo1*, and its role in heart field migration. *robo1* knockdown revealed an unanticipated inhibition of endocardial and myocardial migration (Fig. 3A,B), and many morphant embryos (47%; *n*=108) had unfused heart fields at 20 somites. Unlike *slit2* morphants, which had hyper-migratory endocardial cells with multiple filopodial projections, the endocardial cells in *robo1* morphants exhibited a rounded, non-migratory morphology (Fig. 3A, arrow).

Whereas *Drosophila* have three Robo family members, vertebrates have a fourth, *Robo4*, which is enriched in the endothelium and expressed at low levels in the endocardium in zebrafish (see Fig. S6A,B in the supplementary material). Migration of the heart fields to the midline was not delayed in *robo4* morphants (Fig. 3A). Only 15% of *robo4* morphants (*n*=68) displayed delayed heart field fusion and endocardial cell migration speed was unaffected (Fig. 3B). However, endocardial cell morphology (Fig. 3A) and directionality (Fig. 3C) were affected, suggesting that Robo4 might play a role in heart tube formation. This is consistent with the pericardial edema and circulation defects observed in *robo4* morphants at 48 hpf (see Fig. S3 and Fig. S5A in the supplementary material). The phenotypic differences between *robo1* and *robo4* morphants suggest that these Robo family members have distinct roles in regulating the migration of the heart fields to the midline.

To test the sensitivity of zebrafish heart field migration to Robo1 dosage, we performed Robo1 gain-of-function experiments by injecting rat *Robo1* mRNA (or *mCherry* mRNA as a control) into 1-cell stage embryos and observed heart field migration at 20 somites. Injection of *Robo1* mRNA resulted in incomplete heart field fusion compared with *mCherry* injection [47% of *Robo1* mRNA-injected (*n*=19) versus 15% of *mCherry* mRNA-injected (*n*=13) embryos had delayed fusion; Fig. 4A]. We reasoned that if the *miR-218* morphant phenotype was due, at least in part, to increased Robo1 expression, *robo1* knockdown should rescue the *miR-218* morphant phenotype. Since *robo1* knockdown also

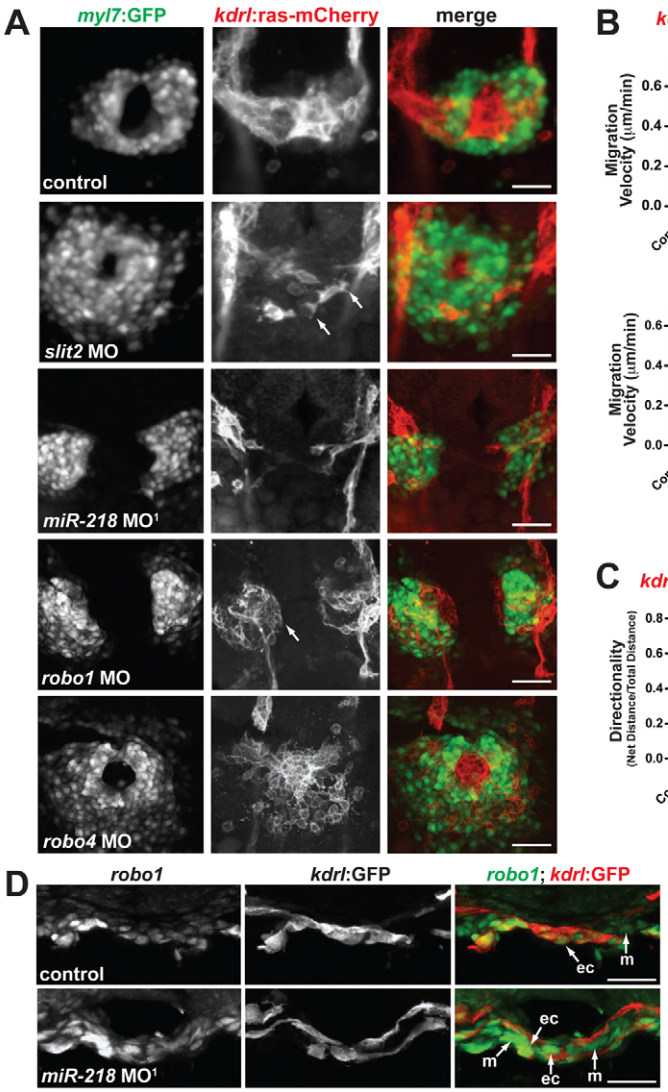

Fig. 3. Slit/Robo signaling regulates heart tube formation. (**A**) Early heart field migration defects in zebrafish morphants: *slit2*, *miR-218*, *robo1* and *robo4*. Shown is *Tg(kdrl*:ras-mCherry*);Tg(myl7*:GFP*)* expression at 20 somites. Dorsal views, anterior to the top. *slit2* morphants have disrupted endocardial migration, including loss of sheet-like migration and endocardial cells have multiple filopodial protrusions (arrows). *miR-218* and *robo1* morphants have delayed migration of the endocardium and myocardium. The endocardial cells of *robo1* morphants display a rounded phenotype (arrow). Migration of the heart fields is not delayed in *robo4* morphants, but the morphology of the endocardial and myocardial cells is altered compared with controls. (**B**) Migration velocities of endocardial [*Tg(kdrl*:ras-mCherry*)* expression] and myocardial [*Tg(myl7*:GFP*)* expression] cells were quantified from time-lapse images. The number of cells tracked is shown above each bar. *slit2* morphants have enhanced endocardial migration rates, whereas *miR-218* and *robo1* have reduced endocardial and myocardial migration rates. *, $P<0.05$ compared with control. (**C**) Directionality of migration was assessed by quantifying the ratio of the net distance traveled to the total distance traveled. A decrease in the ratio indicates an increase in the randomness of migration. *slit2* and *robo4* morphants have defects in directional migration. *, $P<0.05$ compared with control. Data in B and C are mean + s.e.m. (**D**) In situ analysis of *robo1* expression at the 20-somite stage reveals an increase in expression in *miR-218* morphants. Transverse sections, dorsal to the top. ec, endocardium; m, myocardium. Scale bars: 50 μm in A and D.

induced heart field migration defects, we utilized a sub-phenotypic dose of *robo1* MO (1 ng). Whereas *miR-218* knockdown (n=64) delayed heart field migration compared with a control MO (n=71), a combination of a sub-phenotypic dose of *robo1* MO with a phenotypic dose of *miR-218* MO (n=38) significantly rescued the *miR-218* phenotype ($P<0.0001$, Fig. 4B). These results suggest that elevated Robo1 levels are at least partly responsible for the observed heart field migration defects in *miR-218* morphants, perhaps through an increase in Robo1/Slit2 repulsion, and that heart field migration is sensitive to Robo1 dosage.

In a similar fashion, we examined Slit2 gain-of-function in vivo. In control embryos, endocardial cells were arranged in a disc with a core of densely packed cells centered at the embryonic midline (Fig. 4C). However, in embryos overexpressing Slit2-GFP (beginning at the 5-somite stage) endocardial cells did not form a disc at the 20-somite stage, but were mediolaterally diffuse and less densely packed at the midline [70% of Slit2-GFP embryos displayed this phenotype (n=16) compared with 16% of controls (n=12); Fig. 4C]. Endocardial cells also appeared larger and less rounded than in control embryos. These results, combined with the *slit2* knockdown data and *robo1* loss- and gain-of-function data, suggest that the dosage of Slit-Robo signaling components is important in endocardial cell migration.

Vegf signaling controls heart tube fusion and is regulated by Slit/Robo

The migration defects observed in *slit2* morphants led us to hypothesize that the Slit/Robo signaling pathway acts to control the responsiveness of endocardial cells to a midline chemoattractant. Slit2 inhibits Vegf signaling in endothelial cells (Jones et al., 2008; Jones et al., 2009; Marlow et al., 2010) and *vegfa* knockdown induces profound pericardial edema by 48 hpf (Nasevicius et al., 2000). However, it is unclear whether this edema is exclusively attributable to defective angiogenesis from 22 hpf onward, or if Vegf also plays a primary role in cardiac morphogenesis. We therefore examined whether Vegf is involved in recruiting endocardial cells to the midline in zebrafish.

vegfa knockdown delayed heart field fusion in 63% of morphants (n=16). Both endocardial and myocardial cells migrated more slowly in *vegfa* morphants than in controls (Fig. 5A). Transient inhibition of Vegf signaling with a Vegf receptor (Vegfr) inhibitor during heart field migration (14-20 somites; 16-19 hpf), but before the onset of angiogenesis, delayed heart tube fusion at the 20-somite stage [Fig. 5A; 41% of inhibitor-treated embryos had delayed migration (n=17)] and resulted in severe cardiac dysfunction at 48-72 hpf (Fig. 5B). This phenotype occurred in the absence of vascular patterning defects, as the drug was removed

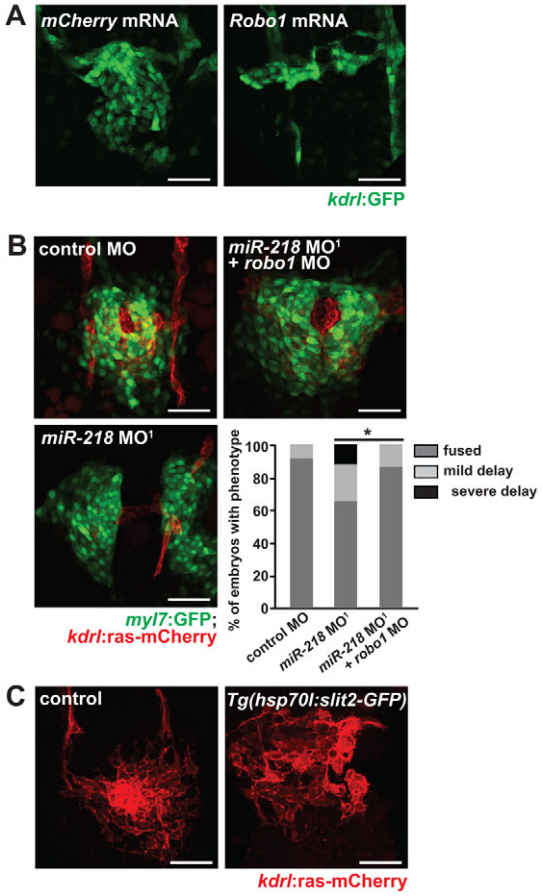

Fig. 4. Heart field migration is sensitive to Robo1 dosage. (**A**) Endocardial migration was defective at 20 somites in zebrafish embryos injected with 75 pg *Robo1* mRNA (*mCherry* mRNA was utilized as a control). (**B**) Rescue of migration defects in *miR-218* morphants was accomplished by co-injecting sub-phenotypic doses of *robo1* MO. Quantification of migration defects is shown beneath. *, $P<0.05$ (Fisher's exact test for a 2×3 contingency table). (**C**) Analysis of endocardial migration at the 20-somite stage in *Tg(hsp70l:slit2-GFP)* embryos that were heat shocked at 5 somites. Embryos lacking the transgene were used as a control. Disorganization of the endocardium was evident in Slit2-overexpressing embryos. Scale bars: 50 μm.

before ISV sprouting. By contrast, continued inhibition of Vegf signaling from 16 to 48 hpf resulted in profound pericardial edema and severe defects in vascular patterning, including a failure to form distinct arterial and venous axial vessels (Fig. 5B). Consistent with an early role for Vegf in cardiac morphogenesis, inhibiting Vegfr after heart tube fusion (24-48 hpf) did not result in edema or cardiac defects, despite obvious angiogenic defects (Fig. 5B). These experiments reveal a temporal window during which Vegf signaling appears to regulate heart formation, prior to its role in blood vessel patterning.

Whereas directional migration was compromised in *slit2* morphant endocardial cells, perhaps owing to enhanced Vegf motogenic activity, *robo1* morphants had reduced endocardial motility. We hypothesized that, in contrast to Robo4, which inhibits Vegf signaling, Robo1 might potentiate the responsiveness of the heart fields to Vegf. We injected sub-phenotypic doses of *vegfa* and *robo1* MOs, either alone or in combination, at the 1- to 2-cell stage and assessed heart field fusion at 20-22 somites (Fig. 5C). At the low doses used, *robo1* or *vegfa* MO alone had only subtle effects on heart field fusion. However, co-injection of sub-phenotypic doses of *robo1* and *vegfa* MOs dramatically increased the percentage of embryos with delayed heart field fusion. In addition, 22% of the co-injected embryos (n=51) had a delayed migration phenotype resembling cardia bifida, compared with only 2.5% of *vegfa*-only (n=40) and no *robo1*-only (n=37) or control MO-injected (n=23) embryos. These results reveal an in vivo interaction between *robo1* and *vegfa* in the regulation of heart field migration.

To determine the mechanisms by which the Slit/miR-218/Robo axis might regulate Vegf signaling, *miR-218* was overexpressed in cultured endothelial cells (HUVEC). In a wound closure assay, *miR-218*-overexpressing cells failed to respond to VEGF-induced migration (Fig. 6A). *miR-218* overexpression also disrupted the polarization of the cells towards the wound edge (Fig. 6B). We next examined MAP kinase pathway activation in response to VEGF stimulation and found that endothelial cells overexpressing *miR-218*, and thus expressing less ROBO1, failed to robustly activate the MAP kinase pathway after VEGF treatment (Fig. 6C). Pretreatment of endothelial cells with recombinant SLIT2-N [the bioactive, N-terminal cleavage fragment of SLIT2 (Nguyen Ba-Charvet et al., 2001)] blunted the VEGF-induced activation of the MAP kinase pathway, and this SLIT-dependent effect was enhanced in *miR-218* mimic-transfected cells (Fig. 6D). *ROBO1* knockdown (Fig. 6E) recapitulated the MAP kinase signaling defect seen in *miR-218*-overexpressing cells, especially in SLIT2-N pretreated cells (Fig. 6F).

Although SLIT2 directly interacts with ROBO1 (Suchting et al., 2005), it is not clear whether SLIT2 directly interacts with ROBO4 (Park et al., 2003; Suchting et al., 2005; Zhang et al., 2009). However, SLIT2 inhibits VEGF signaling through a ROBO4-dependent pathway (Jones et al., 2008; Jones et al., 2009; Marlow et al., 2010), perhaps by binding to a ROBO4 co-receptor, such as ROBO1 or Syndecan (Sheldon et al., 2009). To determine whether ROBO1 promotes VEGF signaling directly or by antagonizing SLIT2/ROBO4 inhibition of VEGF signaling, we knocked down *ROBO4* in HUVEC (Fig. 6E). *ROBO4* knockdown increased VEGF signaling, as reported (Jones et al., 2008; Jones et al., 2009). Combinatorial knockdown of *ROBO1* and *ROBO4* partially rescued the *ROBO1* knockdown signaling defect (Fig. 6F). This result suggests that, although ROBO1 and ROBO4 may compete for SLIT2-dependent pathway activation, ROBO1 also exerts a positive effect on VEGF signaling that is independent of ROBO4.

To determine if ROBO1 downregulation was responsible for the MAP kinase signaling defects in *miR-218*-overexpressing cells, we transfected *Robo1* (lacking the 3′ UTR) into endothelial cells. Exogenous ROBO1 largely rescued the defect in MAP kinase activation in *miR-218*-overexpressing cells and restored VEGF signaling in SLIT2-N-pretreated cells (Fig. 6G). To elucidate how SLIT2/ROBO1 signaling impinges on the VEGF signaling pathway, we examined signaling events proximal to VEGF-induced activation of the VEGF receptor VEGFR2. VEGF-dependent auto-phosphorylation of VEGFR2 (Y1175) was diminished in *ROBO1* knockdown cells, and this effect was even more dramatic in SLIT2-N-treated cells (Fig. 6H). *ROBO4* knockdown did not appear to affect VEGFR2 phosphorylation, in agreement with a previous report (Jones et al., 2008).

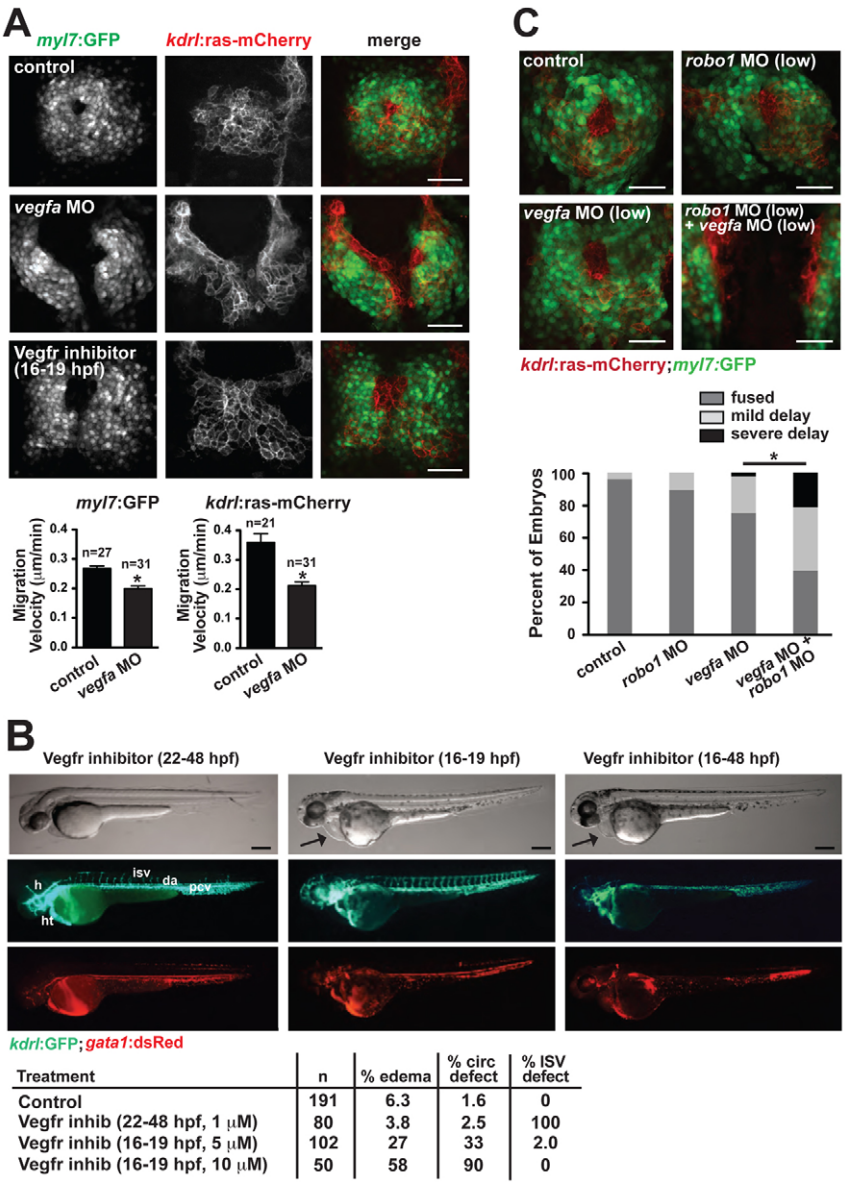

Treatment	n	% edema	% circ defect	% ISV defect
Control	191	6.3	1.6	0
Vegfr inhib (22-48 hpf, 1 μM)	80	3.8	2.5	100
Vegfr inhib (16-19 hpf, 5 μM)	102	27	33	2.0
Vegfr inhib (16-19 hpf, 10 μM)	50	58	90	0

Fig. 5. Vegf regulates the migration of the endocardium/myocardium towards the midline. (**A**) Defects in heart field migration in zebrafish *vegfa* morphants and embryos treated with Vegfr inhibitor (10 μM Vatalanib at 14-20 somites,16-19 hpf). Quantification of migration velocity of the myocardium [*Tg(myl7*:GFP*)* expression] and endocardium [*Tg(kdrl*:ras-mCherry*)* expression] in *vegfa* morphants is indicated beneath. *, $P<0.05$ compared with control. Data are mean + s.e.m. (**B**) The patterning of the intersomitic vessels (ISVs) and the head vasculature is severely disrupted by inhibiting Vegfr after heart field migration has occurred (1 μM Vatalanib at 22-48 hpf, left panels), but pericardial edema does not occur and blood flow through the dorsal aorta and posterior cardinal vein is robust. By contrast, edema (arrow) and circulation defects occur when Vegfr is inhibited during heart field migration (10 μM Vatalanib at 16-19 hpf, middle panels), despite the normal patterning of the vessels after removal of the drug at 19 hpf. Continued inhibition of Vegfr (10 μM Vatalanib from 16-48 hpf, right panels) results in profound edema (arrow), which appears to result from severe vascular defects, including a fused dorsal aorta/posterior cardinal vein. Quantification of circulation phenotypes is shown beneath. A circulation defect was defined as reduced blood flow in the axial vessels. (**C**) Genetic interaction between *vegfa* and *robo1* was assessed by use of sub-phenotypic levels of *vegfa* and *robo1* MOs. The combination of these MOs resulted in profound migration defects observable at the 20-somite stage. Quantification of phenotypes is shown beneath. Mild delay was defined as the contralateral heart fields contacting at the posterior end but remaining unfused anteriorly. Severe delay was defined as a complete absence of heart field fusion at the midline. *, $P<0.05$ (Fisher's exact test for a 2×3 contingency table). h, head; ht, heart; isv, intersomitic vessel; da, dorsal aorta; pcv, posterior cardinal vein. Scale bars: 50 μm in A,C; 100 μm in B.

DISCUSSION

The data presented here indicate that Slit/Robo signaling controls migration of the heart fields to the midline in zebrafish, in part by modulating Vegf signaling in the endocardium (Fig. 7). The titration of Vegf activity may be further refined by miR-218, which is intronically encoded in *slit2* and *slit3* and directly targets *robo1* for repression. This Slit/miR-218/Robo/Vegf feedback regulatory loop provides an elegant mechanism for precise regulation of the migration of the heart fields to form the linear heart tube.

Vegf signaling is tightly regulated in endothelial cells. This regulation includes crosstalk with other signaling pathways, such as Notch and TGFβ (for a review, see Holderfield and Hughes, 2008), as well as Vegf retention in the extracellular matrix (Park et al., 1993; Chen et al., 2010; Purushothaman et al., 2010). Vegf signaling can also be regulated by microRNA-mediated control of signaling molecules that act downstream of the Vegf receptor (Fish et al., 2008; Wang et al., 2008; Nicoli et al., 2010). Our data lend further evidence to a functional interplay between the Slit/Robo pathway and Vegf signaling (Jones et al., 2008). Using temporal inhibition of Vegf activity, we found that Vegf is a mediator of midline heart field migration in zebrafish. We additionally showed that *robo1* and *vegfa* interact in vivo to control heart field migration, and that Robo1 facilitates the phosphorylation of Vegfr2 in response to Vegf. Our data suggest that the *robo1* gene dosage is critical for the proper migration of the heart fields to the midline. Although Robo1 appears to be a positive regulator of Vegf signaling and *robo1* morphants displayed a delayed heart field migration phenotype, the phenotype of *miR-218* morphants and *robo1* mRNA-injected embryos suggests that Robo1 overexpression also causes delayed migration. These data suggest that Robo1/Slit signaling can mediate repulsion during heart field migration. Moreover, although miR-218 may target several genes, we found that the migratory defect in *miR-218* morphants could be rescued by partial *robo1* knockdown, suggesting that *robo1* is a functional target of miR-218.

The expression pattern of Slit/Robo components is complex and not tissue restricted. As Slit2 is a secreted ligand, the Slit/Robo pathway may have multiple cell-autonomous and non-cell-autonomous roles. Our data support the hypothesis that Slit2 expression and secretion from the midline control endocardial

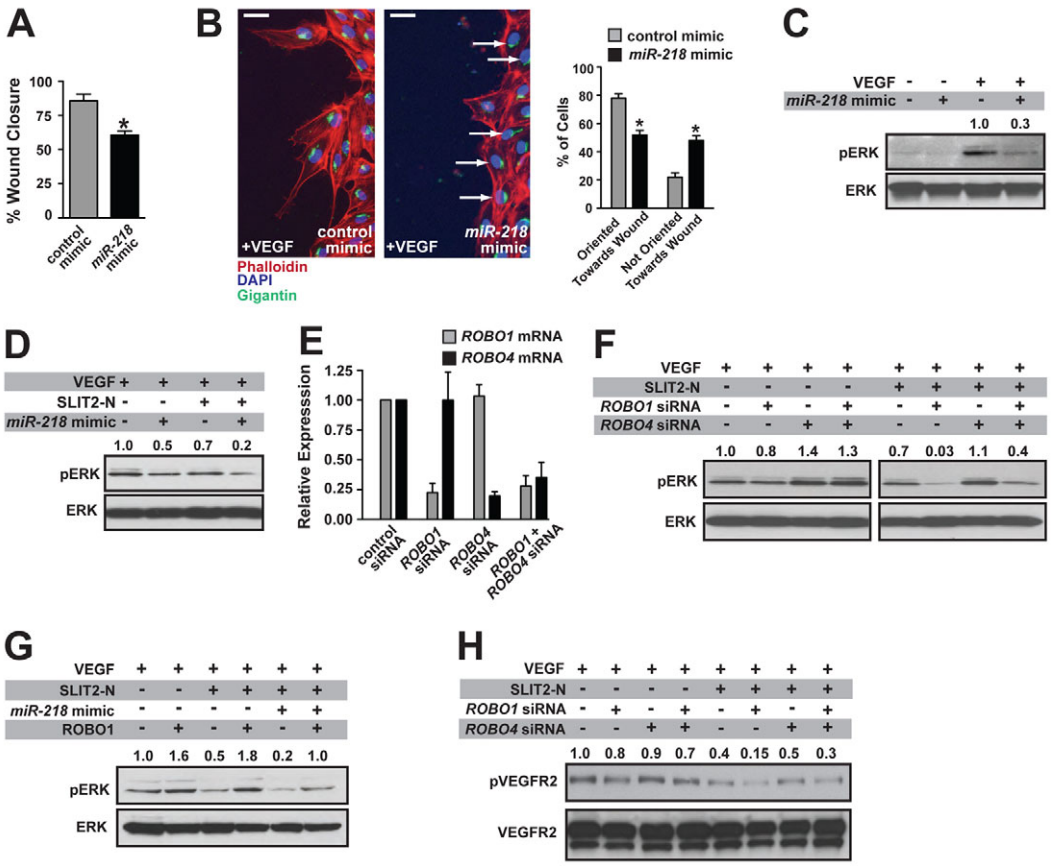

Fig. 6. *miR-218* regulates the response of endothelial cells to VEGF through the regulation of Slit/Robo signaling. (**A**) HUVEC transfected with *miR-218* mimic have reduced VEGF-stimulated migration in a scratch wound assay. Measurements were taken 16 hours after scratch wounding. *, $P<0.05$ compared with control mimic. (**B**) Polarity, assessed by the arrangement of the Golgi apparatus (visualized by Gigantin staining, green) in relation to the scratch surface, was visualized and quantified, demonstrating polarity defects in *miR-218* mimic-transfected cells. Cells were scored as either polarized (Gigantin staining less than 45° from scratch face) or non-polarized (arrows) towards the wound edge. *, $P<0.05$ compared with control mimic. Scale bars: 25 μm. (**C**) Defective MAP kinase signaling in VEGF-treated HUVEC transfected with *miR-218* mimic as determined by blotting for phospho-ERK. Densitometric quantification is shown above the lanes, with the VEGF-treated control sample being set to 1.0. Densitometric values were normalized to that of the loading control. (**D**) Pretreatment of cells with SLIT2-N resulted in increased inhibition of MAP kinase pathway activity in *miR-218*-transfected cells. (**E**) Real-time qRT-PCR confirmed knockdown in *ROBO1* and *ROBO4* in siRNA-transfected cells. (**F**) Defective VEGF-dependent MAP kinase signaling in HUVEC transfected with *ROBO1* siRNA, enhanced MAP kinase signaling with *ROBO4* siRNA, and partial rescue of *ROBO1* siRNA defects with *ROBO4* siRNA, in the presence or absence of SLIT2-N. The left and right panels are from the same blot, with identical exposures. (**G**) Rescue of the MAP kinase signaling defect by overexpression of ROBO1 in *miR-218* mimic-transfected cells. (**H**) Defects in VEGF-dependent phospho-VEGFR2 in *ROBO1* siRNA-transfected cells. Data in A, B and E are mean + s.e.m.

responses to motogenic stimuli such as Vegf. Since Vegf receptors are expressed on endocardial cells (Bussmann et al., 2007), Vegf is likely to signal directly to the endocardium to regulate cell migration to the midline. The defects in myocardial migration in *vegfa* morphants might therefore be due to endocardial-myocardial crosstalk (Holtzman et al., 2007). Since *miR-218* and Slit/Robo components are expressed in the endothelium/endocardium, our data also suggest that Slit/Robo signaling might play a cell-autonomous role within the endocardium to control Vegf responsiveness (Fig. 7). The distinct contributions of autocrine versus paracrine Slit/Robo signaling in the control of heart field migration remain to be determined.

The conserved genomic organization of *Slit2/miR-218-1* and *Slit3/miR-218-2* in vertebrates suggests an important and conserved function for the embedding of this microRNA in the *Slit2/3* genes. Whether a similar Slit/miR-218/Robo signaling network also controls mammalian heart formation remains to be determined; however, a similar regulatory loop appears to control postnatal vascular growth in mice (Small et al., 2010). Interestingly, dynamic regulation of Robo1 is crucial during *Drosophila* development (Kidd et al., 1998b). The *Drosophila* genome does not encode miR-218, but Robo1 expression is controlled by a *Drosophila*-specific protein, Commissureless, that regulates the cell-surface localization of Robo1. Our findings provide insight into how Robo1 titration can be achieved during development in the absence of a vertebrate Commissureless homolog.

In summary, we have elucidated a novel regulatory pathway that controls the migration of the heart fields to the midline in zebrafish. Our findings provide a new paradigm of receptor/ligand regulation, in which a ligand-encoded microRNA regulates the expression of its own receptor. Given the importance of the Slit/Robo pathway in the development and pathology of other organ systems (Kidd et al., 1999; Wu et al., 2001; Wang et al., 2003; Marlow et al., 2010; Tie

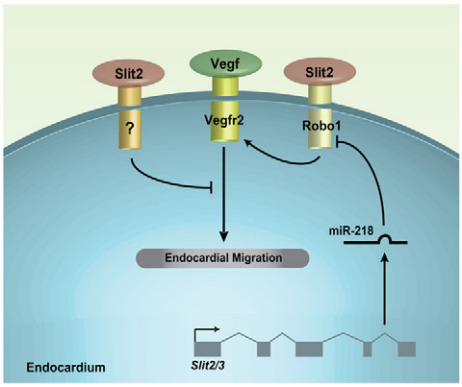

Fig. 7. Model of a Slit/miR-218/Robo axis that regulates Vegf signaling and endocardial migration. Slit2 inhibits the migration of the endocardium to the midline through a combination of negative regulation of the Vegf signaling pathway and Slit/Robo-mediated repulsion signals. During midline migration, the endocardium is likely to sense Slit2 secreted by the floor plate; however, autocrine signaling may also play a role in endocardial migration. The identity of the Slit2 receptor(s) that mediates the negative regulation of Vegf signaling is unclear as this effect appears to be at least partly Robo4 independent. The *Slit2/3*-encoded microRNA miR-218 targets *Robo1* (and *Robo2* and *Srgap2*, not shown) for repression. Robo1 positively regulates endocardial migration, perhaps by promoting the auto-phosphorylation of Vegfr2. However, increased Robo1 expression in *miR-218* morphants may mediate Slit/Robo-mediated repulsion, suggesting that miR-218 might titrate the levels of *Robo1* to facilitate heart field migration.

et al., 2010), our findings are likely to have broad implications for understanding the contribution of the Slit/Robo pathway to the regulation of developmental and pathological processes.

Acknowledgements

We thank Christopher Jones for valuable discussions; the laboratory of Dean Y. Li (University of Utah) for providing protocols and reagents; Ana Ayala and Milly Alva for fish care; Jon Moulton (Gene Tools) for morpholino design; Wendy Staub (Herwig Baier laboratory, UCSF) for technical assistance with microRNA in situs; the Nikon Imaging Center at UCSF for imaging equipment and software; Sheel Dandekar and Orion Weiner (UCSF) for help with image denoising; and Gary Howard and Bethany Taylor for editorial assistance. J.E.F. was supported by postdoctoral fellowships from the Canadian Institute of Health Research and the Heart and Stroke Foundation of Canada; J.D.W. and S.W. were supported by postdoctoral fellowships from the National Institutes of Health (NIH T32HL007731); B.G.B. received funding from NHLBI (P01-HL089707-01A1) and the Lawrence J. and Florence A. DeGeorge Charitable Trust/American Heart Association Established Investigator Award; D.Y.R.S. received funding from the National Institutes of Health (HL54737) and the Packard Foundation; and D.S. received funding from the NHLBI/NIH, the California Institute of Regenerative Medicine and the Younger Family Foundation. Deposited in PMC for release after 12 months.

Competing interests statement

The authors declare no competing financial interests.

Supplementary material

Supplementary material for this article is available at
http://dev.biologists.org/lookup/suppl/doi:10.1242/dev.060046/-/DC1

References

Alexander, J., Rothenberg, M., Henry, G. L. and Stainier, D. Y. (1999). casanova plays an early and essential role in endoderm formation in zebrafish. *Dev. Biol.* **215**, 343-357.

Bedell, V. M., Yeo, S. Y., Park, K. W., Chung, J., Seth, P., Shivalingappa, V., Zhao, J., Obara, T., Sukhatme, V. P., Drummond, I. A. et al. (2005). roundabout4 is essential for angiogenesis in vivo. *Proc. Natl. Acad. Sci. USA* **102**, 6373-6378.

Bussmann, J., Bakkers, J. and Schulte-Merker, S. (2007). Early endocardial morphogenesis requires Scl/Tal1. *PLoS Genet.* **3**, e140.

Chen, T. T., Luque, A., Lee, S., Anderson, S. M., Segura, T. and Iruela-Arispe, M. L. (2010). Anchorage of VEGF to the extracellular matrix conveys differential signaling responses to endothelial cells. *J. Cell Biol.* **188**, 595-609.

Chi, N. C., Shaw, R. M., De Val, S., Kang, G., Jan, L. Y., Black, B. L. and Stainier, D. Y. (2008). Foxn4 directly regulates tbx2b expression and atrioventricular canal formation. *Genes Dev.* **22**, 734-739.

Chung, W. S. and Stainier, D. Y. (2008). Intra-endodermal interactions are required for pancreatic beta cell induction. *Dev. Cell* **14**, 582-593.

Cordes, K. R., Sheehy, N. T., White, M. P., Berry, E. C., Morton, S. U., Muth, A. N., Lee, T. H., Miano, J. M., Ivey, K. N. and Srivastava, D. (2009). miR-145 and miR-143 regulate smooth muscle cell fate and plasticity. *Nature* **460**, 705-710.

D'Amico, L., Scott, I. C., Jungblut, B. and Stainier, D. Y. (2007). A mutation in zebrafish hmgcr1b reveals a role for isoprenoids in vertebrate heart-tube formation. *Curr. Biol.* **17**, 252-259.

Devine, C. A. and Key, B. (2008). Robo-Slit interactions regulate longitudinal axon pathfinding in the embryonic vertebrate brain. *Dev. Biol.* **313**, 371-383.

Fish, J. E., Santoro, M. M., Morton, S. U., Yu, S., Yeh, R. F., Wythe, J. D., Ivey, K. N., Bruneau, B. G., Stainier, D. Y. and Srivastava, D. (2008). miR-126 regulates angiogenic signaling and vascular integrity. *Dev. Cell* **15**, 272-284.

Fricke, C., Lee, J. S., Geiger-Rudolph, S., Bonhoeffer, F. and Chien, C. B. (2001). astray, a zebrafish roundabout homolog required for retinal axon guidance. *Science* **292**, 507-510.

Grieshammer, U., Le M., Plump, A. S., Wang, F., Tessier-Lavigne, M. and Martin, G. R. (2004). SLIT2-mediated ROBO2 signaling restricts kidney induction to a single site. *Dev. Cell* **6**, 709-717.

Holderfield, M. T. and Hughes, C. C. (2008). Crosstalk between vascular endothelial growth factor, notch, and transforming growth factor-beta in vascular morphogenesis. *Circ. Res.* **102**, 637-652.

Holmes, G. and Niswander, L. (2001). Expression of slit-2 and slit-3 during chick development. *Dev. Dyn.* **222**, 301-307.

Holtzman, N. G., Schoenebeck, J. J., Tsai, H. J. and Yelon, D. (2007). Endocardium is necessary for cardiomyocyte movement during heart tube assembly. *Development* **134**, 2379-2386.

Huang, C. J., Tu, C. T., Hsiao, C. D., Hsieh, F. J. and Tsai, H. J. (2003). Germ-line transmission of a myocardium-specific GFP transgene reveals critical regulatory elements in the cardiac myosin light chain 2 promoter of zebrafish. *Dev. Dyn.* **228**, 30-40.

Hutson, L. D. and Chien, C. B. (2002). Pathfinding and error correction by retinal axons: the role of astray/robo2. *Neuron* **33**, 205-217.

Jin, S. W., Herzog, W., Santoro, M. M., Mitchell, T. S., Frantsve, J., Jungblut, B., Beis, D., Scott, I. C., D'Amico, L. A., Ober, E. A. et al. (2007). A transgene-assisted genetic screen identifies essential regulators of vascular development in vertebrate embryos. *Dev. Biol.* **307**, 29-42.

Jones, C. A., London, N. R., Chen, H., Park, K. W., Sauvaget, D., Stockton, R. A., Wythe, J. D., Suh, W., Larrieu-Lahargue, F., Mukouyama, Y. S. et al. (2008). Robo4 stabilizes the vascular network by inhibiting pathologic angiogenesis and endothelial hyperpermeability. *Nat. Med.* **14**, 448-453.

Jones, C. A., Nishiya, N., London, N. R., Zhu, W., Sorensen, L. K., Chan, A. C., Lim, C. J., Chen, H., Zhang, Q., Schultz, P. G. et al. (2009). Slit2-Robo4 signalling promotes vascular stability by blocking Arf6 activity. *Nat. Cell Biol.* **11**, 1325-1331.

Kent, W. J., Sugnet, C. W., Furey, T. S., Roskin, K. M., Pringle, T. H., Zahler, A. M. and Haussler, D. (2002). The human genome browser at UCSC. *Genome Res.* **12**, 996-1006.

Kervrann, C. and Boulanger, J. (2006). Optimal spatial adaptation for patch-based image denoising. *IEEE Trans. Image Process.* **15**, 2866-2878.

Kidd, T., Brose, K., Mitchell, K. J., Fetter, R. D., Tessier-Lavigne, M., Goodman, C. S. and Tear, G. (1998a). Roundabout controls axon crossing of the CNS midline and defines a novel subfamily of evolutionarily conserved guidance receptors. *Cell* **92**, 205-215.

Kidd, T., Russell, C., Goodman, C. S. and Tear, G. (1998b). Dosage-sensitive and complementary functions of roundabout and commissureless control axon crossing of the CNS midline. *Neuron* **20**, 25-33.

Kidd, T., Bland, K. S. and Goodman, C. S. (1999). Slit is the midline repellent for the robo receptor in Drosophila. *Cell* **96**, 785-794.

Kupperman, E., An, S., Osborne, N., Waldron, S. and Stainier, D. Y. (2000). A sphingosine-1-phosphate receptor regulates cell migration during vertebrate heart development. *Nature* **406**, 192-195.

Lee, J. S., Ray, R. and Chien, C. B. (2001). Cloning and expression of three zebrafish roundabout homologs suggest roles in axon guidance and cell migration. *Dev. Dyn.* **221**, 216-230.

Li, H. S., Chen, J. H., Wu, W., Fagaly, T., Zhou, L., Yuan, W., Dupuis, S., Jiang, Z. H., Nash, W., Gick, C. et al. (1999). Vertebrate slit, a secreted ligand for the transmembrane protein roundabout, is a repellent for olfactory bulb axons. *Cell* **96**, 807-818.

Liu, J., Zhang, L., Wang, D., Shen, H., Jiang, M., Mei, P., Hayden, P. S., Sedor, J. R. and Hu, H. (2003). Congenital diaphragmatic hernia, kidney agenesis and

cardiac defects associated with Slit3-deficiency in mice. *Mech. Dev.* **120**, 1059-1070.
Marlow, R., Binnewies, M., Sorensen, L. K., Monica, S. D., Strickland, P., Forsberg, E. C., Li, D. Y. and Hinck, L. (2010). Vascular Robo4 restricts proangiogenic VEGF signaling in breast. *Proc. Natl. Acad. Sci. USA* **107**, 10520-10525.
Medioni, C., Astier, M., Zmojdzian, M., Jagla, K. and Semeriva, M. (2008). Genetic control of cell morphogenesis during Drosophila melanogaster cardiac tube formation. *J. Cell Biol.* **182**, 249-261.
Nasevicius, A., Larson, J. and Ekker, S. C. (2000). Distinct requirements for zebrafish angiogenesis revealed by a VEGF-A morphant. *Yeast* **17**, 294-301.
Nguyen Ba-Charvet, K. T., Brose, K., Ma, L., Wang, K. H., Marillat, V., Sotelo, C., Tessier-Lavigne, M. and Chedotal, A. (2001). Diversity and specificity of actions of Slit2 proteolytic fragments in axon guidance. *J. Neurosci.* **21**, 4281-4289.
Nicoli, S., Standley, C., Walker, P., Hurlstone, A., Fogarty, K. E. and Lawson, N. D. (2010). MicroRNA-mediated integration of haemodynamics and Vegf signalling during angiogenesis. *Nature* **464**, 1196-1200.
Ober, E. A., Olofsson, B., Makinen, T., Jin, S. W., Shoji, W., Koh, G. Y., Alitalo, K. and Stainier, D. Y. (2004). Vegfc is required for vascular development and endoderm morphogenesis in zebrafish. *EMBO Rep.* **5**, 78-84.
Osborne, N., Brand-Arzamendi, K., Ober, E. A., Jin, S. W., Verkade, H., Holtzman, N. G., Yelon, D. and Stainier, D. Y. (2008). The spinster homolog, two of hearts, is required for sphingosine 1-phosphate signaling in zebrafish. *Curr. Biol.* **18**, 1882-1888.
Park, J. E., Keller, G. A. and Ferrara, N. (1993). The vascular endothelial growth factor (VEGF) isoforms: differential deposition into the subepithelial extracellular matrix and bioactivity of extracellular matrix-bound VEGF. *Mol. Biol. Cell* **4**, 1317-1326.
Park, K. W., Morrison, C. M., Sorensen, L. K., Jones, C. A., Rao, Y., Chien, C. B., Wu, J. Y., Urness, L. D. and Li, D. Y. (2003). Robo4 is a vascular-specific receptor that inhibits endothelial migration. *Dev. Biol.* **261**, 251-267.
Purushothaman, A., Uyama, T., Kobayashi, F., Yamada, S., Sugahara, K., Rapraeger, A. C. and Sanderson, R. D. (2010). Heparanase-enhanced shedding of syndecan-1 by myeloma cells promotes endothelial invasion and angiogenesis. *Blood* **115**, 2449-2457.
Qian, L., Liu, J. and Bodmer, R. (2005). Slit and Robo control cardiac cell polarity and morphogenesis. *Curr. Biol.* **15**, 2271-2278.
Sakaguchi, T., Kikuchi, Y., Kuroiwa, A., Takeda, H. and Stainier, D. Y. (2006). The yolk syncytial layer regulates myocardial migration by influencing extracellular matrix assembly in zebrafish. *Development* **133**, 4063-4072.
Santiago-Martinez, E., Soplop, N. H., Patel, R. and Kramer, S. G. (2008). Repulsion by Slit and Roundabout prevents Shotgun/E-cadherin-mediated cell adhesion during Drosophila heart tube lumen formation. *J. Cell Biol.* **182**, 241-248.
Schoenebeck, J. J., Keegan, B. R. and Yelon, D. (2007). Vessel and blood specification override cardiac potential in anterior mesoderm. *Dev. Cell* **13**, 254-267.
Sheldon, H., Andre, M., Legg, J. A., Heal, P., Herbert, J. M., Sainson, R., Sharma, A. S., Kitajewski, J. K., Heath, V. L. and Bicknell, R. (2009). Active involvement of Robo1 and Robo4 in filopodia formation and endothelial cell motility mediated via WASP and other actin nucleation-promoting factors. *FASEB J.* **23**, 513-522.
Siepel, A., Bejerano, G., Pedersen, J. S., Hinrichs, A. S., Hou, M., Rosenbloom, K., Clawson, H., Spiethe, J., Hillier, L. W. et al. (2005). Evolutionarily conserved elements in vertebrates, insect, worm and yeast genomes. *Genome Res.* **15**, 1034-1050.
Small, E. M., Sutherland, L., Rajagopalan, K., Wang, S. and Olson, E. N. (2010). MicroRNA-218 regulates vascular patterning by modulation of Slit-Robo signaling. *Circ. Res.* **107**, 1336-1344.
Stein, E. and Tessier-Lavigne, M. (2001). Hierarchical organization of guidance receptors: silencing of netrin attraction by slit through a Robo/DCC receptor complex. *Science* **291**, 1928-1938.
Strickland, P., Shin, G. C., Plump, A., Tessier-Lavigne, M. and Hinck, L. (2006). Slit2 and netrin 1 act synergistically as adhesive cues to generate tubular bi-layers during ductal morphogenesis. *Development* **133**, 823-832.
Suchting, S., Heal, P., Tahtis, K., Stewart, L. M. and Bicknell, R. (2005). Soluble Robo4 receptor inhibits in vivo angiogenesis and endothelial cell migration. *FASEB J.* **19**, 121-123.
Sweetman, D., Rathjen, T., Jefferson, M., Wheeler, G., Smith, T. G., Wheeler, G. N., Munsterberg, A. and Dalmay, T. (2006). FGF-4 signaling is involved in mir-206 expression in developing somites of chicken embryos. *Dev. Dyn.* **235**, 2185-2191.
Tie, J., Pan, Y., Zhao, L., Wu, K., Liu, J., Sun, S., Guo, X., Wang, B., Gang, Y., Zhang, Y. et al. (2010). MiR-218 inhibits invasion and metastasis of gastric cancer by targeting the Robo1 receptor. *PLoS Genet.* **6**, e1000879.
Traver, D., Paw, B. H., Poss, K. D., Penberthy, W. T., Lin, S. and Zon, L. I. (2003). Transplantation and in vivo imaging of multilineage engraftment in zebrafish bloodless mutants. *Nat. Immunol.* **4**, 1238-1246.
Trinh, L. A. and Stainier, D. Y. (2004). Fibronectin regulates epithelial organization during myocardial migration in zebrafish. *Dev. Cell* **6**, 371-382.
Wang, B., Xiao, Y., Ding, B. B., Zhang, N., Yuan, X., Gui, L., Qian, K. X., Duan, S., Chen, Z., Rao, Y. et al. (2003). Induction of tumor angiogenesis by Slit-Robo signaling and inhibition of cancer growth by blocking Robo activity. *Cancer Cell* **4**, 19-29.
Wang, S., Aurora, A. B., Johnson, B. A., Qi, X., McAnally, J., Hill, J. A., Richardson, J. A., Bassel-Duby, R. and Olson, E. N. (2008). The endothelial-specific microRNA miR-126 governs vascular integrity and angiogenesis. *Dev. Cell* **15**, 261-271.
Wu, J. Y., Feng, L., Park, H. T., Havlioglu, N., Wen, L., Tang, H., Bacon, K. B., Jiang, Z., Zhang, X. and Rao, Y. (2001). The neuronal repellent Slit inhibits leukocyte chemotaxis induced by chemotactic factors. *Nature* **410**, 948-952.
Yeo, S. Y., Miyashita, T., Fricke, C., Little, M. H., Yamada, T., Kuwada, J. Y., Huh, T. L., Chien, C. B. and Okamoto, H. (2004). Involvement of Islet-2 in the Slit signaling for axonal branching and defasciculation of the sensory neurons in embryonic zebrafish. *Mech. Dev.* **121**, 315-324.
Zhang, B., Dietrich, U. M., Geng, J. G., Bicknell, R., Esko, J. D. and Wang, L. (2009). Repulsive axon guidance molecule Slit3 is a novel angiogenic factor. *Blood* **114**, 4300-4309.